PCCP

COMMUNICATION

View Article Online
View Journal | View Issue

Cite this: *Phys. Chem. Chem. Phys.*, 2018, **20**, 7407

Received 26th January 2018,
Accepted 21st February 2018

DOI: 10.1039/c8cp00590g

rsc.li/pccp

Optical spectroscopy of isolated flavins: photodissociation of protonated lumichrome†

Alexander Sheldrick, David Müller, Alan Günther, Pablo Nieto and Otto Dopfer *

The optical properties of flavins strongly depend on the charge and oxidation states as well as the environment. Herein, the electronic spectrum of cold protonated lumichrome, the smallest flavin molecule, is recorded by means of photodissociation in the visible range (VISPD) in a cryogenic ion trap tandem mass spectrometer coupled to an electrospray ionization source. The vibronic spectrum is assigned to the $S_1 \leftarrow S_0$ ($\pi\pi^*$) transition of the most stable N5-protonated isomer by comparison with quantum chemical calculations at the PBE0/cc-pVDZ level in combination with multi-dimensional Franck–Condon simulations. Analysis of the geometric and electronic structures of neutral and protonated lumichrome explains the large red shift of the band origin upon protonation ($\Delta S_1 \sim -6000$ cm^{-1}), which corresponds to the increase in proton affinity upon S_1 excitation as a result of charge transfer. N5 protonation greatly modifies the structure of the central pyrazine ring of the chromophore. The orbitals involved in $S_1 \leftarrow S_0$ excitation include an important fraction of the probability at the central ring and they are, hence, largely influenced by the positive charge of the attached proton. The rich vibronic spectrum indicates the large geometry change upon S_1 excitation. This combined experimental and computational approach is shown to be suitable to determine the optical properties of flavins as a function of oxidation, protonation, metalation, and microsolvation state.

1. Introduction

Flavins are a family of yellow bioorganic dye molecules derived from the 7,8-dimethyl-10-alkylisoalloxazine chromophore (isolumichrome = iso-LC for R = H). Due to the ability of the chromophore to absorb in a wide spectral range, flavins play a vital role in many biological processes.[1,2] Flavins only differ by the substituent (R) attached to the N10 position of the chromophore (Fig. 1). The most prominent members of the flavin family include lumichrome (LC, no substituent at N10 but H at N1), lumiflavin (LF, R = methyl), riboflavin (RF, R = ribityl, vitamin B_2), and flavin mononucleotide (FMN, R = ribophosphate). The range of the absorption sensitively depends on the substituent, the protonation, metalation, and oxidation state, as well as the solvent environment. Thus, the absorption spectrum has been shown to be a valuable indicator to determine changes in the electronic structure of the flavin.[2–8] The ability of flavins to serve as electron donors and acceptors depending on environment and their wide absorption bands have made them an integral part of many biological processes.[2] Examples of the latter have been found in fungi, where flavins act as blue light receptors or as light sensory modules in plants and bacteria.[9,10] Their potential as redox reaction partners has also been studied in the respiratory chain[11] and in the repair of DNA.[12] They are also the most important components of flavoproteins, where they occur as catalyst in the oxidation of glucose by GOx enzymes.[11,13]

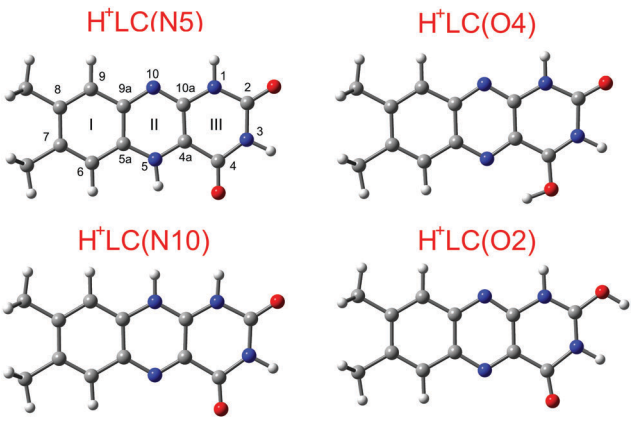

Fig. 1 Lowest-energy structural isomers of protonated lumichrome (H^+LC) calculated at the PBE0/cc-pVDZ level. Atomic and ring numbers are indicated for H^+LC(N5) according to IUPAC notation.

Technische Universität Berlin, Institut für Optik und Atomare Physik, Hardenbergstr. 36, Berlin D-10623, Germany. E-mail: dopfer@physik.tu-berlin.de; Fax: +49 30 314 23018

† Electronic supplementary information (ESI) available. See DOI: 10.1039/c8cp00590g

The photochemical properties of flavins has been the subject of extensive research since their structure was determined by chemical synthesis more than 80 years ago.[14,15] In fact, the Nobel prize in chemistry in 1937 was awarded to Paul Karrer for his pioneering investigations on flavins.[16] Most of the studies on flavins and their complexes has been carried out in solution.[4–8,11] There is, however, some question on the considerable influence of both solvent and counter ions on the flavin properties.[4–8,11] Hence, spectroscopic experiments on flavin molecules and their aggregates isolated in the gas phase are required to obtain information about the intrinsic structural, electronic, and chemical properties of the optically active species. To this end, basic properties, such as their geometric and electronic structure, stability, and their interaction with the solvent must be characterized at the molecular level. However, due to their difficult generation in the gas phase, experiments on isolated flavins have been extremely rare. The few available studies include a fluorescence spectrum of LF embedded in superfluid He droplets,[17] the determination of the proton and electron affinities of LF by mass spectrometry,[18] and the photo- and collision-induced fragmentation of protonated FMN.[19] Very recently, the optical spectrum and fragmentation pattern of flavin adenine dinucleotide anions (FAD^-) has been reported.[20] The FAD^- spectrum recorded at room temperature shows a rather broad ($\sim$100 nm) band centered around 440 nm and does not provide any structural information. The preferred metalation site and binding energy of alkali and coinage metal ions attached to LC[21] and LF[22] in the ground electronic state (S_0) has recently been determined in our group by infrared multiphoton dissociation (IRMPD) spectroscopy in a room temperature ion trap and quantum chemical calculations at the B3LYP/cc-pVDZ level. Similarly, the preferred protonation site in the S_0 state of several isolated flavins, including LC, LF, RF, and FMN, was determined at room temperature using the same experimental and computational approach.[23] The determined protonation site strongly depends on the substituent, and for protonated lumichrome (H^+LC) the analysis of the IRMPD spectrum revealed the N5 position as the most stable protonation site. No evidence was obtained for other less favorable protonation sites and the presence of iso-LC protomers, although theory predicts them to be low in energy (Table 1).[23]

Table 1 Proton affinities (PA) and relative energies (ΔE_0) in kJ mol^{-1} calculated at the PBE0/cc-pVDZ level compared to corresponding values determined at the B3LYP/cc-pVDZ level

	PBE0/cc-pVDZ		B3LYP/cc-pVDZ[a]	
Isomer	PA	ΔE_0	PA	ΔE_0
LC		0		0
iso-LC		54.9		53.5
H^+LC(N5)	930.6	0	935.0	0
H^+LC(O4)	911.3	19.3	914.2	20.8
H^+LC(N10)	899.1	31.5	904.3	30.7
H^+LC(O2)	861.1	69.5	865.7	69.3
H^+iso-LC(O4)	926.5	59.0	930.0	58.5
H^+iso-LC(N5)	907.2	78.3	912.2	76.3

[a] Ref. 23.

Although the optical absorption properties of isolated flavin ions are of paramount importance for understanding many biochemical processes, they are completely unexplored. The case of LC as the smallest representative of the flavin class of molecules is particularly interesting. The lowest optical excitation was predicted to be a dark $n\pi^*$ transition, and only higher-energy bright $\pi\pi^*$ transitions were observed in the liquid phase.[24] Protonation of LC is expected to have a substantial effect on its electronic structure and molecular orbitals. Hence, large electronic shifts upon protonation are expected in the absorption spectrum of LC. The detailed analysis of these effects is the aim of the present investigation. We combine electrospray ionization with cryogenic ion trapping to characterize cold H^+LC ions in the gas phase *via* optical photodissociation spectroscopy in the visible range (VISPD) performed in a tandem mass spectrometer. The vibronic spectrum, along with a very brief preliminary analysis, was presented in an earlier report to illustrate of the capabilities of the recently constructed cryogenic ion trap spectrometer (BerlinTrap).[25] While vibrational IR spectroscopy of large biomolecular ions can readily be performed at room temperature without substantial loss in spectral resolution, cooling down to low temperature is definitively required for optical spectroscopy in order to avoid hot band transitions leading to spectral congestion,[25–33] in the worst case leading to unresolved vibronic fine structure. Significantly, the VISPD spectrum of cold H^+LC ions corresponds to the first optical spectrum of any flavin molecule recorded in the gas phase.[25] Herein, we present the detailed analysis of the experimental spectrum through comparison with quantum chemical simulations. To this end, density functional theory (DFT) calculations for the electronic structure of the lowest electronic states are combined with multidimensional Franck–Condon (FC) simulations to assign the observed vibronic spectrum. The computational analysis provides details of the geometrical, vibrational, and electronic properties of the ground, first, and second excited singlet states of H^+LC (S_n, n = 0–2). Comparison with LC reveals the large effects of protonation on the electronic structure of this simplest flavin molecule.

2. Experimental and computational details

A detailed description of the employed experimental apparatus (BerlinTrap) employed for VISPD spectroscopy of H^+LC has been given elsewhere.[25] Briefly, the central parts of the BerlinTrap setup include (i) an electrospray ionization (ESI) source to generate ions, (ii) a quadrupole mass spectrometer to size-select the desired ions, (iii) a cryogenic 22-pole ion trap to store and cool the ions *via* He buffer gas, and (iv) a reflectron time-of-flight mass spectrometer (ReTOF-MS) to analyze the product ions. H^+LC ions are generated in the ESI source by spraying a LC-containing solution at a 2 mL h^{-1} rate. The analyte solution consists of 2 mg LC (Sigma Aldrich, >99% purity), 17 mL MeOH, and 2.5 mL formic acid. H^+LC ions are then mass selected (m/z 243) and guided *via* several linear RF multipoles to a 22-pole trap, where they are stored for 90 ms and cooled down to 25 K by means of He buffer gas cooling.

After extraction from the trap, the cold H^+LC ions are irradiated at the extraction region of the orthogonal ReTOF-MS, and both fragment and parent ions are simultaneously detected using a microchannel plate detector. Laser radiation is provided by a commercial optical parametric oscillator (OPO) laser system (Continuum, Panther EX-OPO) pumped by the third harmonic of a Nd:YAG laser (Continuum, Powerlite DLS 9010). Typical OPO laser intensities are 3–5 mJ per pulse at an area of around 2 cm^2. The laser wavelength (bandwidth 2–3 cm^{-1}) is tuned in 0.02 nm steps and calibrated with a grating spectrometer (Bristol Instruments, 821). The mass discriminated ion signals registered at the microchannel plate are digitalized and converted to action spectra *via* homemade LabVIEW programs. The VISPD spectra are obtained by adding the acquired fragment signals and linear normalization by both parent ion signal and laser intensity. In this way, VISPD spectra of H^+LC are recorded in the 19 700–20 800 cm^{-1} spectral range.

DFT calculations at the PBE0/cc-pVDZ level are carried out for the optimization of the ground states for LC, iso-LC, H^+LC, and H^+iso-LC using GAUSSIAN09.[34] The PBE0 functional is employed as a computationally economic method, because it shows good results as found by Medvedev *et al.*[35] who compared various levels of theory to the computationally more expensive CCSD level. Furthermore, the PBE0 data agree well with the structures and energies obtained at the B3LYP level previously used for the IR spectroscopic characterization of flavin ions[21–23] but yields much better predictions for excited state energies with respect to adiabatic electronic transitions and vibronic bands. Vertical excitation energies are calculated with the time-dependent DFT (TD-DFT) method at the optimized ground state geometry. Geometries of the excited electronic states are optimized at the same level of theory using the corresponding ground state structures as the starting point. The natural transition orbital method[36] is used to calculate the orbitals involved in the lowest electronic excitations. Calculated proton affinities and relative energies are corrected for harmonic zero-point vibrational energies. Vibronic spectra based on multidimensional FC simulations are simulated for T = 0 K using PGOPHER.[37] The resulting stick spectra are convoluted with a Lorentzian line profile using a FWHM of 6 cm^{-1} to facilitate convenient comparison with the experimental VISPD spectrum.

3. Results and discussion

A variety of low-energy H^+LC and iso-H^+LC isomers with different protonation sites are considered to assign the measured VISPD spectrum.[23] The proton may attach to the various available nucleophilic sites of LC (Fig. 1) and iso-LC (Fig. S1 in ESI†), such as the lone pairs of the O atoms of the two CO groups (denoted O2 and O4) and the lone pairs of the two heterocyclic N atoms (N10 and N5 for LC, N5 and N1 for iso-LC). LC is calculated to be ΔE_0 = 54.9 kJ mol^{-1} more stable than iso-LC. As a result, only the formation of H^+LC may be expected. However, iso-H^+LC may still be present in solution because of solvent stabilization effects and thus they may also be generated in the ESI source. In our previous IRMPD experiments on M^+LC ions produced by ESI, isomers with relative free energies as high as 37 kJ mol^{-1} were identified.[21] Therefore, the most stable N5 and O4 isomers of H^+iso-LC are also considered here. The calculated proton affinities (PA) and relative energies (ΔE_0) of all considered H^+(iso-)LC isomers in Table 1 show good agreement between the PBE0 and B3LYP levels.[23] H^+LC(N5) is the global minimum structure, corresponding to PA = 930.6 kJ mol^{-1}. The other three O4, N10, and O2 isomers of H^+LC have relative energies of ΔE_0 = +19.3, +31.5, and +69.5 kJ mol^{-1}, respectively. Although the H^+iso-LC and H^+LC isomers have somewhat different PAs for the same protonation site, the relative energies of all H^+iso-LC isomers are still relatively high, with ΔE_0 = +59.0 and +78.3 kJ mol^{-1} for the O4 and N5 isomers of H^+iso-LC, because of the large energy gap between the two neutral molecules.

The VISPD spectrum of the $S_1 \leftarrow S_0$ transition of H^+LC recorded between 19 700 and 20 800 cm^{-1} is obtained by monitoring the two predominant fragment ion signals (m/z 172 and 198, Fig. S2 in ESI†), linearly normalized for laser power and parent ion intensity (m/z 243). The range close to the adiabatic S_1 origin transition is plotted in Fig. 2, while a larger range is shown in Fig. S3 in ESI.† No VISPD signal is observed down to 19 600 cm^{-1}. The action spectra recorded in both fragment channels are essentially the same (Fig. S4 in ESI†), which provides a first hint (but no proof) that the observed spectrum is produced by a single isomer. The branching ratio is around 3 : 1 for m/z 198 and 172. The same major fragment ions are observed for IRMPD activation,[23] which indicates that optical activation into the S_1 state is followed by internal conversion to the S_0 ground electronic state and subsequent statistical dissociation. The m/z 198 fragment ion corresponds to formal loss of CO + NH_3 or HCN + H_2O, whereas the m/z 172 ion arises from formal loss of CONH + CO.[23] The 22-pole trap temperature is kept at 25 K to maximize the VISPD signal. This temperature is low enough to minimize the appearance of hot bands, which are below the

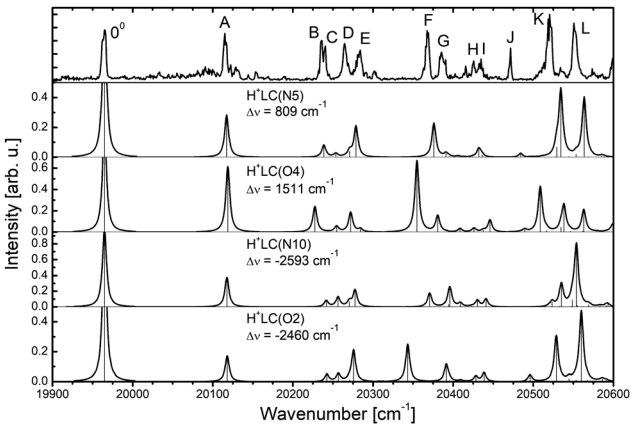

Fig. 2 Comparison between experimental VISPD spectrum recorded for H^+LC and Franck–Condon simulations for the isomers shown in Fig. 1 calculated at the PBE0/cc-pVDZ level using a convolution width of 6 cm^{-1}. Isomers are ordered from top to bottom according to their relative energy (Table 1). The energy scale of the simulated spectra is shifted by $\Delta\nu$ to match the frequencies of calculated and observed S_1 origins at 19 962 cm^{-1}.

detection limit. The S_1 band origin is recorded at 19 962 cm^{-1}. Toward higher frequency, many intense vibronic transitions (labeled A–L in Fig. 2) are observed, which indicate a large geometry change upon electronic excitation. The measured bands have a width of around 6 cm^{-1} (FWHM), which is composed of the laser bandwidth ($\sim$2–3 cm^{-1}) and unresolved rotational structure. The measured spectrum reveals a substantial redshift of the first electronic transition of H^+LC compared to that of neutral LC. Although no experimental data are available for isolated LC, the maximum of its first absorption band in solution was found to be in the 379–385 nm range ($\sim$26 000 cm^{-1}) depending on the solvent.[24] Thus, the large red shift of around -6000 cm^{-1} demonstrates that protonation of the aromatic chromophore strongly changes both its geometric and electronic configuration.

To determine the isomer observed in the experimental spectrum, we consider next to the proton affinities also the positions of the adiabatic $S_1 \leftarrow S_0$ origin transitions and the vibronic spectra simulated within the Franck–Condon approximation. The resulting vibronic spectra are compared to the measured VISPD spectrum in Fig. 2 for the considered H^+LC isomers and in Fig. S5 in ESI† for the iso-H^+LC isomers. For convenient comparison between experimental and computed vibronic spectra, the computed spectra are shifted in these figures by a constant amount ($\Delta\nu$) to match the calculated and experimental S_1 origins, $\Delta\nu = S_1^{exp} - S_1^{calc}$ with S_1^{exp} = 19 962 cm^{-1}. All adiabatic S_1 energies are listed in Table 2, along with the corresponding $\Delta\nu$ shifts. From this comparison, the observed VISPD spectrum is clearly assigned to the $S_1 \leftarrow S_0$ transition of the most stable H^+LC(N5) isomer. First, considering the absolute position of the predicted S_1 origins, the best match with the observed value is obtained for H^+LC(N5), with a deviation of only $\Delta\nu$ = 809 cm^{-1}. The comparison is much less favorable for all other isomers of both H^+LC ($\Delta\nu$ = 1511, -2593, -2460 cm^{-1} for O4, N10, O2) and iso-H^+LC ($\Delta\nu$ = 2408 and 4525 cm^{-1} for O4 and N5). Second, also the vibronic pattern predicted for H^+LC(N5) shows the best agreement with the experimental spectrum with respect to both position and relative intensity of the transitions. In particular, H^+LC(N5) is the only isomer able to reproduce the high intensity doublet K and L at around 20 550 cm^{-1}, thus confirming the assignment of the observed VISPD spectrum to the $S_1 \leftarrow S_0$ transition of H^+LC(N5). The observed deviations between experimental and computed vibronic intensities may arise from several factors, including deficiencies in the electronic structure calculations, deviations from the harmonic FC principle, vibronic coupling, and mode-dependent dissociation cross sections and competing radiative and nonradiative relaxation channels. The assignment to the N5 isomer confirms the conclusion obtained from our previous IRMPD experiments combined with B3LYP/cc-pVDZ calculations.[23]

After identification of H^+LC(N5) as carrier of the observed VISPD spectrum, we consider in Fig. 3 and Table 3 in more detail the assignment of the vibrational transitions. A full set of normal modes for the S_0 and S_1 states of H^+LC(N5) can be found in Table S1 in the ESI.† The notation of the vibrations follows the Mullikan convention. The $S_1 \leftarrow S_0$ transition has $\pi\pi^*$ character and the N5 isomer belongs to the C_s point group. Therefore, all vibronic transitions originating from the ground vibrational level in the S_0 electronic state terminate in S_1 vibrational states with a' symmetry. The agreement between experimental and calculated vibrational frequencies is very good. The maximum and mean deviations of 12 and 4 cm^{-1}, respectively, are small considering the experimental peak width (6 cm^{-1}) and the harmonic approximation employed for the FC analysis. Most of the vibronic transitions are fundamentals of the lowest frequency a′ modes of H^+LC(N5), 44^1–53^1, and only fundamentals, overtones, and combination bands of these in-plane modes are observed. Graphical representations of these normal coordinates are given in Fig. S6 in ESI.† Briefly, bands A and D are identified as short progression in mode 53 with one and two quanta, respectively. This mode involves in-plane bending of the outer aromatic rings I and III around the central ring II. The B/C doublet is assigned to in-plane rocking modes of the methyl groups attached to C7 (mode 52) and C8 (mode 51). Both modes also include the shear deformation of ring II along the N5–N10 direction. Mode 50 (band E) involves a uniform stretching of the three chromophore rings along the long molecular axis. Mode 49 (band F) is described by the compression of ring III combined with the scissoring motion of the two carbonyl groups. Combination bands 53^152^1 and 53^150^1 are assigned to bands G and H, respectively. Band G also contains a minor contribution of the 48^1 fundamental associated with a shear deformation of ring I along the C6–C9 axis. A hindered rotation

Table 2 Adiabatic S_1 energies of LC and various isomers of H^+LC and H^+iso-LC calculated at the PBE0/cc-pVDZ level, along with the shifts from the experimental S_1 origin of H^+LC (in cm^{-1})

Isomer	S_1	$\Delta\nu$
LC	24 826	
H^+LC (exp)	19 962	0
H^+LC(N5)	19 153	809
H^+LC(O4)	18 451	1511
H^+LC(N10)	22 555	−2593
H^+LC(O2)	22 422	−2460
H^+iso-LC(O4)	17 554	2408
H^+iso-LC(N5)	15 437	4525

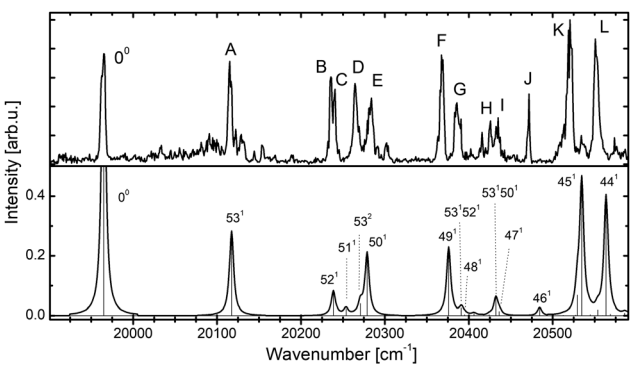

Fig. 3 Experimental VISPD spectrum of H^+LC (top) compared to the Franck–Condon simulation of the identified H^+LC(N5) isomer (bottom) along with vibrational assignments (Table 3).

Table 3 Experimental frequencies for vibronic transitions observed in the VISPD spectrum of the S_1 state of H^+LC compared to frequencies of the H+LC(N5) isomer computed at the PBE0/cc-pVDZ level, along with the mode assignment

Band	ν (exp.)	ν (calc.)	Assignment
	19 962	19 153	0^0
A	+154	153.1	53^1
B	+274	273.9	52^1
C	+278	289.0	51^1
D	+303	306.2	53^2
E	+321	314.7	50^1
F	+406	411.7	49^1
G	+425	427.0	53^152^1
		430.8	48^1
H	+464	467.8	53^150^1
I	+473	471.5	47^1
J	+509	519.9	46^1
K	+558	569.8	45^1
L	+590	598.6	44^1

of the rigid ring II (mode 47), and the elongation of ring III along the N1–C4 axis combined with the elongation of rings I and II along the long molecular axis (mode 46), are assigned to bands I and J, respectively. Two complex delocalized deformation modes of all three rings are attributed to the very intense bands K (45^1) and L (44^1). The intensities for most vibronic transitions are well reproduced by the FC simulations. Nevertheless, the intensities calculated for all transitions involving vibrations 52, 51, and 46 are slightly underestimated. There are also a number of reproducible low-intensity bands around transition A that could not be explained by the FC simulations. All obvious efforts to rationalize these transitions by hot bands using FC simulations at finite temperature or by other isomers failed.

The structures calculated for LC in the S_0 and S_1 states are given in Fig. S7 (ESI†), while the S_0 geometry of H^+LC(N5) is shown in Fig. S8 in ESI.† The relative changes of the geometry induced by N5 protonation of LC in the S_0 state are visualized in Fig. 4(a). Positive numbers imply distance elongation upon protonation, while negative numbers indicate distance contraction. Although the excess positive charge has an influence throughout the whole chromophore, the most prominent feature is a compression of ring II along the N5–N10 axis (−8.3 pm), along with an elongation of the same ring along the C5a–C10a axis (6.7 pm). Ring III is also contracted noticeably along the C2–C4a distance (−6.1 pm). In contrast, a relatively smaller deformation is induced in ring I. N5 protonation also affects the length of the C2O (−1.2 pm) and C4O (0.5 pm) bonds of the two carbonyl groups. The latter effect is used in previous studies as sensitive indicator for determination of the protonation site by means of IRMPD spectroscopy and B3LYP calculations of the C=O stretch fundamentals.[23]

The geometry change upon $S_1 \leftarrow S_0$ electronic excitation of H^+LC(N5) is shown in Fig. 4(b) and will be used to rationalize the relative FC intensities of the simulated and observed vibronic transitions. Electronic excitation has an even more drastic effect on the geometry of the chromophore than protonation. The consequences of electronic excitation are substantial throughout the whole chromophore, and are particularly strong in rings I

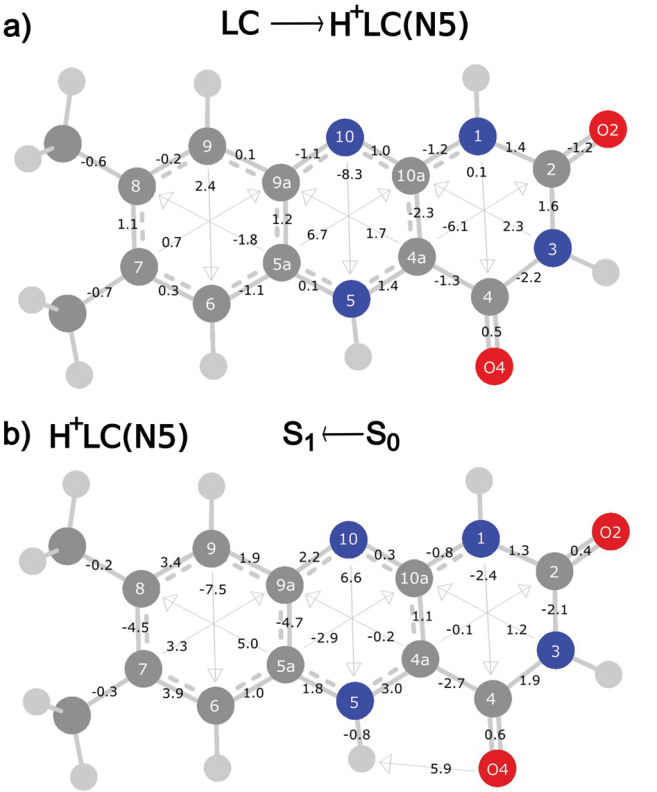

Fig. 4 (a) Relative structural changes (in pm) of H^+LC(N5) with respect to neutral LC in the ground electronic state (S_0) to illustrate the structural effects of protonation. Positive values indicate elongation upon protonation. (b) Relative structural changes (in pm) of the S_1 state with respect to the S_0 state of H^+LC(N5) to illustrate the structural effects of electronic ππ* excitation. Positive values indicate elongation upon excitation. Absolute geometries are available in Fig. S7 and S8 in ESI.†

and II. In this case, the expansion of ring II along the N5–N10 axis (6.6 pm) is accompanied by a compression of the same ring along the C5a–C10a axis (−2.9 pm). Ring I is greatly contracted along the C9–C6 distance (−7.5 pm) and expanded along the C7–C9a (3.3 pm) and the C8–C5a (5.0 pm) directions. In contrast, only a smaller deformation is induced in ring III, with a contraction along the N1–C4 axis (−2.4 pm) and an elongation of the N3–C10a distance (1.2 pm). $S_1 \leftarrow S_0$ excitation also moderately affects the length of the C2O (0.4 pm) and C4O (0.6 pm) bonds to the two carbonyl groups. The deformation induced by $S_1 \leftarrow S_0$ excitation is very similar to the 45 normal mode of the S_1 state. Therefore, a large FC factor is expected for this fundamental, and the associated band K assigned to 45^1 is indeed the most intense vibronic transition in both the experimental and simulated VISPD spectrum in Fig. 2. Similarly, the modes 49 and 50 also include a compression of ring I, which explains their high FC factors and the large intensities of the corresponding bands F and E, respectively.

In a next step, we consider the nature of the lowest electronic singlet excitations in LC and H^+LC(N5). The energies and oscillator strengths (f) for the first two vertical transitions originating from their optimized S_0 ground state geometries are listed in Table 4. For all but one transition, adiabatic

Table 4 Transition energies ($\Delta\nu$) and oscillator strengths (f) for the vertical (adiabatic) transitions originating from the electronic ground state of LC and H^+LC(N5) calculated at the PBE0/cc-pVDZ level

Isomer	Transition	$\Delta\nu$ [cm^{-1}]	f ($\times 10^{-3}$)
LC	$S_1 \leftarrow S_0$ ($n\pi^*$)	28 213 (24 826)	1.3
	$S_2 \leftarrow S_0$ ($\pi\pi^*$)	28 745 (—)[a]	86.4
H^+LC(N5)	$S_1 \leftarrow S_0$ ($\pi\pi^*$)	22 026 (19 153)	47.7
	$S_2 \leftarrow S_0$ ($n\pi^*$)	25 696 (20 767)	0.3

[a] All efforts to optimize this state failed.

energies are given as well. The orbitals involved in these $S_1 \leftarrow S_0$ and $S_2 \leftarrow S_0$ transitions are shown in Fig. 5. In agreement with previous calculations,[24] the lowest excited singlet state (S_1) of LC corresponds to a very weak $n\pi^*$ excitation from HOMO to LUMO at 28 213 cm^{-1} ($f = 1.3 \times 10^{-3}$). Very close in energy at 28 745 cm^{-1} is the optically bright S_2 state arising from $\pi\pi^*$ excitation (HOMO−1 to LUMO) with $f = 86 \times 10^{-3}$. For this reason, only the $S_2 \leftarrow S_0$ transition of LC is observed in solution near ~380 nm (~26 000 cm^{-1}),[24] with the band maximum depending somewhat on the solvent. For H^+LC(N5), the energy order of $\pi\pi^*$ and $n\pi^*$ excitation changes (Table 4), and the optically bright $\pi\pi^*$ transition ($f = 48 \times 10^{-3}$) becomes the lowest singlet excited state (S_1) at 22 026 cm^{-1}, while the dark $n\pi^*$ state (S_2) is much higher in energy (25 696 cm^{-1}, $f = 0.3 \times 10^{-3}$). As a result, the computed red shift in the vertical excitation energy for the $\pi\pi^*$ state upon protonation (−6719 cm^{-1}) is much larger than that for the $n\pi^*$ state (−2517 cm^{-1}). The experimental red shift observed for the $\pi\pi^*$ transition is of the order of −6000 cm^{-1}, in excellent agreement with the theoretical predictions. Large shifts upon protonation of aromatic molecules were observed previously, providing that protonation occurs at the aromatic chromophore.[38] Since all orbitals involved in S_1 and S_2 excitation of LC and H^+LC(N5) involve electron density near N5 (Fig. 5), a considerable electronic shift is expected for both transitions upon N5 protonation. However, the n orbital (HOMO) is clearly influenced to a larger extent than the π orbital (HOMO−1), because the former is mostly localized at the central ring II, whose geometry is greatly modified upon N5 protonation. In contrast, a large part of the HOMO−1 orbital is localized at ring I that is less affected by N5 protonation, as discussed above. Thus, from the shapes of the orbitals, one can readily rationalize that for H^+LC(N5) the $n\pi^*$ transition is more than 3000 cm^{-1} higher in energy than the $\pi\pi^*$ transition.

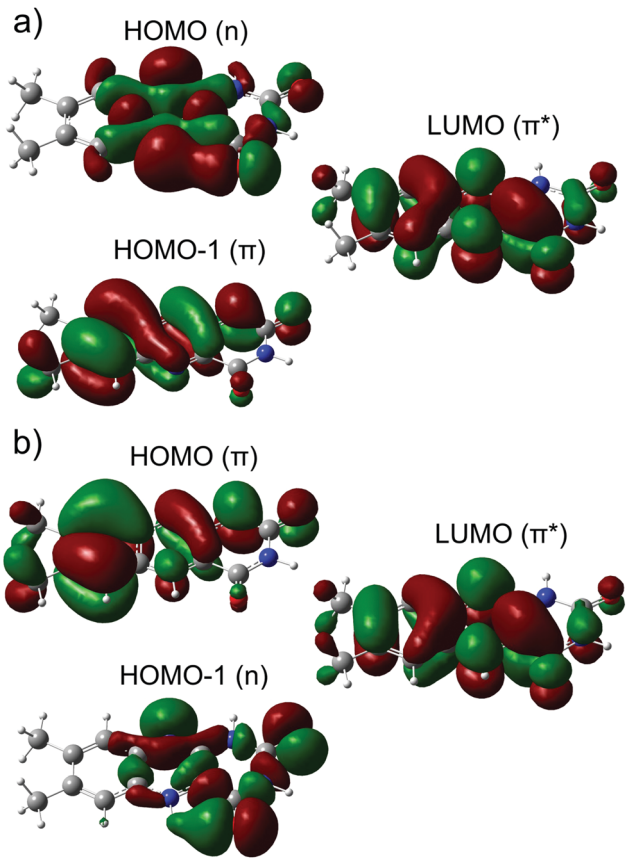

Fig. 5 Molecular orbitals involved in the $S_1 \leftarrow S_0$ (LUMO ← HOMO, $n\pi^*$) and $S_2 \leftarrow S_0$ (LUMO ← HOMO−1, $\pi\pi^*$) transitions of LC (a) compared to those of the corresponding $S_1 \leftarrow S_0$ (LUMO ← HOMO, $\pi\pi^*$) and $S_2 \leftarrow S_0$ (LUMO ← HOMO−1, $n\pi^*$) transitions of H^+LC(N5) (b), respectively (TD-DFT, PBE0/cc-pVDZ).

4. Concluding remarks

We report the first optical spectrum of a flavin molecule isolated in the gas phase. The electronic spectrum of the $S_1 \leftarrow S_0$ ($\pi\pi^*$) transition of protonated lumichrome (H^+LC), the simplest member of the flavin family, is obtained by photodissociation spectroscopy in the visible range near 500 nm, with an S_1 origin located at 19 962 cm^{-1}. The VISPD spectrum is recorded in a recently commissioned cryogenic ion trap tandem mass spectrometer coupled to an electrospray ionization source (BerlinTrap), suitable for spectroscopy of cryogenic biomolecular ions and their clusters.[25] Cooling the ions down to temperatures below 30 K ensures the absence of hot band transitions and thus yields a vibrationally resolved electronic spectrum of the first excited singlet state. The analysis of the measured vibronic spectrum using TD-DFT calculations coupled to multidimensional FC simulations provides a reliable structural, vibrational, and electronic assignment, and the salient results may be summarized as follows.

(1) The carrier of the observed VISPD spectrum is the most stable H^+LC(N5) isomer, in line with the thermochemical predictions and the analysis of the IRMPD spectrum recorded at room temperature.[23] There is no indication for the contribution of other less stable isomers to the VISPD spectrum in this spectral range. (2) The S_1 state of H^+LC(N5) is assigned to optically bright $\pi\pi^*$ excitation. S_1 excitation has a large effect on the structure of the aromatic chromophore, leading to intense and rich vibronic activity according to the FC principle. All FC-allowed low-frequency fundamentals are identified in the VISPD spectrum, and their excitation is correlated with the calculated geometry change. (3) N5 protonation of LC induces a drastic change in both its geometry and electronic structure. In particular, the bright $\pi\pi^*$ state experiences a rather large red shift of around −6000 cm^{-1} (30%) upon protonation from the broad absorption of LC in the

liquid phase ($\sim$380 nm, $\sim$26 000 cm^{-1}).[24] This large shift is readily rationalized by the strong interaction of the proton directly attached to the central ring of the aromatic chromophore with the orbitals involved in the transition and the resulting charge transfer.[38] In particular, the energy of the LUMO (π^*) is strongly lowered, giving rise to the large red shift of the $\pi\pi^*$ state. Because the close lying optically dark $n\pi^*$ state of LC is significantly less affected by N5 protonation, the energetic order of the two lowest electronic singlet states ($n\pi^*$, $\pi\pi^*$) changes between LC and H^+LC(N5). Similar large red shifts in electronic excitations upon protonation have been reported for other aromatic molecules, in which the proton is directly attached to the aromatic chromophore (*e.g.*, naphthalene)[38,39] and not to the side chain (*e.g.*, amino acids).[40]

As a more general conclusion, the analysis of the first optical spectrum of an isolated flavin molecule (here protonated lumichrome) illustrates that their intrinsic optical properties depend extremely sensitively on external perturbations (here protonation). The developed combined spectroscopic and computational approach is demonstrated to be a powerful tool to characterize these effects at the molecular level with high spectroscopic precision. Thus, cryogenic ion trap spectroscopy combined with quantum chemical calculations offers the opportunity to unravel the individual impact of oxidation, charge state, metalation, counter ions, and stepwise microsolvation on the photochemical properties of this fundamental class of biomolecules, thereby improving our molecular-level understanding of biochemical processes involving flavins. Currently, this strategy is applied to larger protonated[23] and metalated[21,22] flavins to probe the perturbation of the electronic structure as a function of the flavin substituent, and the charge, type, binding site, and bond strength of the metal ion.

Conflicts of interest

There are no conflicts to declare.

Acknowledgements

This work was supported by Deutsche Forschungsgemeinshaft (DFG, grant number DO 729/6). We thank Dieter Gerlich, TU Chemnitz, and Deutsche Forschungsgemeinschaft for the generous continuous loan of the ESI source, the 22-pole trap, and several turbomolecular pumps.

References

1 P. F. Heelis, *Chem. Soc. Rev.*, 1982, **11**, 15.
2 *Flavins: Photochemistry and Photobiology*, ed. E. Silva and A. M. Edwards, RSC Pub., Cambridge, UK, 2006.
3 W. J. Rutter, *Acta Chem. Scand.*, 1958, **12**, 438.
4 M. Benecky, T. Y. Yu, K. L. Watters and J. T. McFarland, *Biochim. Biophys. Acta*, 1980, **626**, 197.
5 J. Lauterwein, P. Hemmerich and J. M. Lhoste, *Inorg. Chem.*, 1975, **14**, 2152.
6 J. Lauterwein, P. Hemmerich and J. M. Lhoste, *Inorg. Chem.*, 1975, **14**, 2161.
7 F. Müller, P. Hemmerich and A. Ehrenberg, *Eur. J. Biochem.*, 1968, **5**, 158.
8 P. Hemmerich and J. Lauterwein, in *The Structure and Reactivity of Flavin-Metal Complexes*, ed. G. L. Eichhorn, Elsevier Scientific Pub. Co, Amsterdam, London, New York, 1973.
9 A. Losi and W. Gartner, *Photochem. Photobiol.*, 2011, **87**, 491.
10 T. E. Swartz, T. S. Tseng, M. A. Frederickson, G. Paris, D. J. Comerci, G. Rajashekara, J. G. Kim, M. B. Mudgett, G. A. Splitter, R. A. Ugalde, F. A. Goldbaum, W. R. Briggs and R. A. Bogomolni, *Science*, 2007, **317**, 1090.
11 V. Massey, *Biochem. Soc. Trans.*, 2000, **28**, 283.
12 M. Sugiyama, *Environ. Health Perspect.*, 1991, **92**, 63.
13 V. Piano, B. A. Palfey and A. Mattevi, *Trends Biochem. Sci.*, 2017, **42**(6), 457.
14 R. Kuhn and F. Weygand, *Ber. Dtsch. Chem. Ges. B*, 1934, **67**, 2084.
15 P. Karrer, K. Schopp and F. Benz, *Helv. Chim. Acta*, 1935, **18**, 426.
16 *Nobel Lectures: Chemistry 1922–1941*, Elsevier Publishing Company, Amsterdam, 1966.
17 A. Vdovin, A. Slenczka and B. Dick, *Chem. Phys.*, 2013, **422**, 195.
18 T. Zhang, K. Papson, R. Ochran and D. P. Ridge, *J. Phys. Chem. A*, 2013, **117**, 11136.
19 L. Guyon, T. Tabarin, B. Thuillier, R. Antoine, M. Broyer, V. Boutou, J. P. Wolf and P. Dugourd, *J. Chem. Phys.*, 2008, **128**, 75103.
20 M. H. Stockett, *Phys. Chem. Chem. Phys.*, 2017, **19**, 25829.
21 A. Günther, P. Nieto, G. Berden, J. Oomens and O. Dopfer, *Phys. Chem. Chem. Phys.*, 2014, **16**, 14161.
22 P. Nieto, A. Günther, G. Berden, J. Oomens and O. Dopfer, *J. Phys. Chem. A*, 2016, **120**, 8297.
23 J. Langer, A. Günther, S. Seidenbecher, G. Berden, J. Oomens and O. Dopfer, *ChemPhysChem*, 2014, **15**, 2550.
24 E. Sikorska, I. V. Khmelinskii, W. Prukała, S. L. Williams, M. Patel, D. R. Worrall, J. L. Bourdelande, J. Koput and M. Sikorski, *J. Phys. Chem. A*, 2004, **108**, 1501.
25 A. Günther, P. Nieto, D. Müller, A. Sheldrick, D. Gerlich and O. Dopfer, *J. Mol. Spectrosc.*, 2017, **332**, 8.
26 E. Garand, M. Z. Kamrath, P. A. Jordan, A. B. Wolk, C. M. Leavitt, A. B. McCoy, S. J. Miller and M. A. Johnson, *Science*, 2012, **335**, 694.
27 I. Alata, J. Bert, M. Broquier, C. Dedonder, G. Feraud, G. Grégoire, S. Soorkia, E. Marceca and C. Jouvet, *J. Phys. Chem. A*, 2013, **117**, 4420.
28 E. K. Campbell, M. Holz, D. Gerlich and J. P. Maier, *Nature*, 2015, **523**, 322.
29 J. G. Redwine, Z. A. Davis, N. L. Burke, R. A. Oglesbee, S. A. McLuckey and T. S. Zwier, *Int. J. Mass Spectrom.*, 2013, **348**, 9.
30 A. B. Wolk, C. M. Leavitt, E. Garand and M. A. Johnson, *Acc. Chem. Res.*, 2014, **47**, 202.
31 J. Roithová, A. Gray, E. Andris, J. Jašík and D. Gerlich, *Acc. Chem. Res.*, 2016, **49**, 223.

32 K. R. Asmis and J. Sauer, *Mass Spectrom. Rev.*, 2007, **26**, 542.
33 T. R. Rizzo, J. A. Stearns and O. V. Boyarkin, *Int. Rev. Phys. Chem.*, 2009, **28**, 481.
34 M. J. Frisch, G. W. Trucks, H. B. Schlegel, G. E. Scuseria, M. A. Robb, J. R. Cheeseman, G. Scalmani, V. Barone, B. Mennucci and G. A. Petersson, *et al.*, *Gaussian 09, Revision D.01*, Wallingford CT, 2009.
35 M. G. Medvedev, I. S. Bushmarinov, J. Sun, J. P. Perdew and K. A. Lyssenko, *Science*, 2017, **355**, 49.
36 R. L. Martin, *J. Chem. Phys.*, 2003, **118**, 4775.
37 C. M. Western, *J. Quant. Spectrosc. Radiat. Transfer*, 2017, **186**, 221.
38 I. Alata, R. Omidyan, M. Broquier, C. Dedonder, O. Dopfer and C. Jouvet, *Phys. Chem. Chem. Phys.*, 2010, **12**, 14456.
39 U. J. Lorenz, N. Solca, J. Lemaire, P. Maitre and O. Dopfer, *Angew. Chem., Int. Ed.*, 2007, **46**, 6714.
40 O. V. Boyarkin, S. R. Mercier, A. Kamariotis and T. R. Rizzo, *J. Am. Chem. Soc.*, 2006, **128**, 2816.

